Two-photon laser spectroscopy of the gas boundary layer in crossed evanescent and volume waves

V. G. Bordo,[1,2] J. Loerke,[3] L. Jozefowski,[1,*] and H.-G. Rubahn[1]
[1]*Fysisk Institut, Odense Universitet, DK-5230 Odense M, Denmark*
[2]*Institute of General Physics, Russian Academy of Sciences, 117942 Moscow, Russia*
[3]*Max-Planck-Institut für Strömungsforschung, Bunsenstrasse 10, D-37073 Göttingen, Germany*
(Received 29 November 2000; published 7 June 2001)

A spectroscopic approach to the scattering dynamics in the gas-surface boundary layer is presented. The technique utilizes excitation of the vapor atoms in two crossed laser fields, one of which is directed normally to the surface while the other one excites an evanescent wave propagating along the surface. We provide a rigorous and quantitative theoretical description of these two-photon evanescent-volume wave spectra and apply it to the model system of sodium atoms colliding with a dielectric prism surface. A comparison with experimental results reveals quantitative agreement between theory and experiment. We demonstrate that one can distinguish by pure optical means between different groups of atoms, namely atoms moving to the surface and apart from it after being specularly or diffusively scattered. We also extract the two-dimensional velocity distributions of both the arriving and departing groups of atoms.

DOI: 10.1103/PhysRevA.64.012903 PACS number(s): 34.50.Dy, 42.50.−p, 42.62.Fi, 39.30.+w

I. INTRODUCTION

The boundary layer is of key importance for the physical and chemical dynamics of gas-solid interactions ranging from extremely low pressures in an ultrahigh-vacuum environment up to atmospheric pressures. Adsorption and desorption processes are often limiting stages for surface chemical reactions. Laser-induced interface phenomena also depend to a great extent on the relaxation of the excited gas in the boundary layer. In order to control such processes but also in order just to learn how the gas interacts with the surface, one has to distinguish between the gas flux arriving at the surface and the one departing from it. For equilibrium conditions, however, this goal seemed to be unachievable since [1] ‘‘ . . . we are aware of the fact that we will never be able to make the demonstration in a direct experiment under rigorous equilibrium conditions, simply because we cannot distinguish the desorbing molecules under such conditions.’’ For this reason, most of the studies of gas-surface scattering have been carried out with atomic or molecular beams, which obviously do not represent an equilibrium gas. Conventional optical techniques also fail because the signal from the boundary layer is negligibly small as compared to the competing one from the gas volume.

In the present work, we demonstrate that the use of evanescent waves (EW's) can provide a valid way out of this dilemma. They propagate along the gas-solid interface with an amplitude that is maximum at the surface, whereas it rapidly decreases with increasing distance from it [2,3]. EW's can be excited in total internal reflection at a transparent dielectric surface or as surface polaritons [4] on a metal or a semiconductor surface. If the depth of EW penetration into the gas is less than the mean free path of the gas molecules, one encounters a situation similar to the excitation of a molecular beam near a surface. On the other hand, the time of flight of the gas atoms or molecules across the EW field can be less than the radiative relaxation times in the gas volume. Under such conditions, the optical response of the boundary layer becomes essentially transient [5]. In other words, the polarization of the gas is not adapted to the external electric field and is determined by the gas-surface scattering [6–9]. This effect has been demonstrated for the fluorescence spectrum of Na atoms excited by an EW at a glass prism surface [10]. A two-photon fluorescence spectrum excited by two counterpropagating EW's has been shown to be very sensitive to the velocity distribution function of the atoms leaving the surface [11]. This made it possible to confirm Knudsen's cosine law by spectroscopic means.

The spectroscopic possibilities of EW excitation can be largely increased if one excites the boundary layer by a volume wave (VW) traveling along the normal to the surface. Due to the different Doppler shifts for atoms moving to the surface and apart from it, one can discriminate between their contributions. Now, combining evanescent and volume wave excitation in a two-photon excitation scheme, one can spectrally distinguish between the atoms just before they collide with the surface and just after they left it. The Doppler-broadened two-photon line shape will then be determined by the *two-dimensional* velocity distribution functions of both the atoms arriving at the surface and departing from it and thus will contain information about the dynamics of the gas-solid scattering [12]. In the present work, we demonstrate this idea for a model system consisting of sodium vapor near a glass prism surface.

II. THEORY

A. Optical Bloch equations

The evolution of the atom interacting with the external fields is described by the Liouville equation for the atomic density matrix $\rho(\mathbf{r},\mathbf{v},t)$,

$$\left(\frac{\partial}{\partial t}+\mathbf{v}\cdot\boldsymbol{\nabla}\right)\rho=-\frac{i}{\hbar}[H_0+V,\rho]-\Gamma\rho, \tag{1}$$

*On leave from Marian Smoluchowski Institute of Physics, Jagiellonian University, ul. Reymonta 4, 30-059 Cracow, Poland.

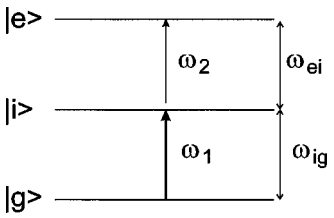

FIG. 1. Notation of the atomic levels and the exciting laser frequencies.

where the vector **r** determines the position of an atom with respect to the interface and **v** is its velocity, H_0 is the Hamiltonian of the free atom, and Γ is the relaxation operator. In the dipole approximation, the interaction operator V can be written as

$$V=-\mu[\mathbf{E}_1(\mathbf{r})\cos(\omega_1 t-\mathbf{k}_1\cdot\mathbf{r})+\mathbf{E}_2(\mathbf{r})\cos(\omega_2 t-\mathbf{k}_2\cdot\mathbf{r})], \tag{2}$$

where μ is the dipole moment operator, and $\mathbf{E}_i(\mathbf{r})$, ω_i, and $\mathbf{k}_i$ are the amplitude, frequency, and wave vector of the corresponding electromagnetic wave, respectively. The evanescent character of the wave implies that

$$\mathbf{E}_i(\mathbf{r})=\mathbf{E}_i\exp(-\kappa_i z), \tag{3}$$

where $\kappa_i=\delta_i^{-1}$ and δ_i is the penetration depth of the EW into the gas; the z axis is chosen along the normal to the interface towards the gas interior. The EW wave vector is directed along the interface and this direction is chosen as the x axis. For the volume wave, its amplitude is supposed to be independent of the position of the atom and its wave vector is parallel to the z axis.

We consider the case in which wave 1 is resonant with the transition between the ground atomic state $|g\rangle$ and the intermediate excited state $|i\rangle$, whereas wave 2 is resonant with the transition between the state $|i\rangle$ and the upper excited state $|e\rangle$ (Fig. 1). We shall analyze two excitation configurations: (i) the lower transition is excited by a volume wave, whereas the upper transition is scanned by an evanescent wave (the so-called ''normal configuration'') [Fig. 2(a)]; (ii) the lower transition is excited by an evanescent wave, whereas the upper transition is scanned by a volume wave (the ''inverse configuration'') [Fig. 2(b)].

Let us introduce the substitutions,

$$\rho_{ig}=\exp[-i(\omega_1 t-\mathbf{k}_1\cdot\mathbf{r})]\sigma_{ig}, \tag{4}$$

$$\rho_{ei}=\exp[-i(\omega_2 t-\mathbf{k}_2\cdot\mathbf{r})]\sigma_{ei}, \tag{5}$$

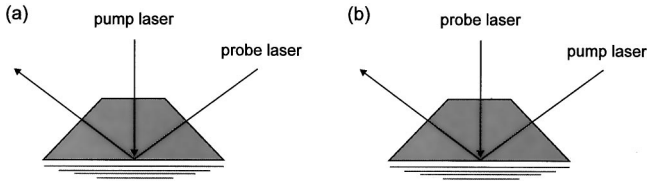

FIG. 2. The two investigated laser-prism geometries for fluorescence excitation: the ''normal'' (a) and the ''inverse'' (b) configuration. The gas atoms collide with the prism from the bottom.

$$\rho_{eg}=\exp\{-i[(\omega_1+\omega_2)t-(\mathbf{k}_1+\mathbf{k}_2)\cdot\mathbf{r}]\}\sigma_{eg}, \tag{6}$$

$$\rho_{jj}=\sigma_{jj}\quad(j=g,i,e) \tag{7}$$

and perform the rotating-wave approximation. In the steady-state limit (both on t and x), we get the following equations [13]:

$$v_z\frac{d\sigma_{gg}}{dz}=\gamma_i\sigma_{ii}+\frac{i}{2}\Omega_1(z)(\sigma_{ig}-\sigma_{gi}), \tag{8}$$

$$v_z\frac{d\sigma_{ii}}{dz}=-\gamma_i\sigma_{ii}+\gamma_e\sigma_{ee}+\frac{i}{2}\Omega_1(z)(\sigma_{gi}-\sigma_{ig})+\frac{i}{2}\Omega_2(z)\times(\sigma_{ei}-\sigma_{ie}), \tag{9}$$

$$v_z\frac{d\sigma_{ee}}{dz}=-\gamma_e\sigma_{ee}+\frac{i}{2}\Omega_2(z)(\sigma_{ie}-\sigma_{ei}), \tag{10}$$

$$v_z\frac{d\sigma_{ig}}{dz}=(i\tilde{\Delta}_1-\gamma_{ig})\sigma_{ig}+\frac{i}{2}\Omega_1(z)(\sigma_{gg}-\sigma_{ii})+\frac{i}{2}\Omega_2(z)\sigma_{eg}, \tag{11}$$

$$v_z\frac{d\sigma_{ei}}{dz}=(i\tilde{\Delta}_2-\gamma_{ei})\sigma_{ei}-\frac{i}{2}\Omega_1(z)\sigma_{eg}+\frac{i}{2}\Omega_2(z)(\sigma_{ii}-\sigma_{ee}), \tag{12}$$

$$v_z\frac{d\sigma_{eg}}{dz}=(i\tilde{\Delta}_0-\gamma_{eg})\sigma_{eg}-\frac{i}{2}\Omega_1(z)\sigma_{ei}+\frac{i}{2}\Omega_2(z)\sigma_{ig}, \tag{13}$$

with the Rabi frequencies of the corresponding transitions,

$$\Omega_1(z)=\frac{\mu_{ig}\mathbf{E}_1}{\hbar}\exp(-\kappa_1 z)=\Omega_1\exp(-\kappa_1 z), \tag{14}$$

$$\Omega_2(z)=\frac{\mu_{ei}\mathbf{E}_2}{\hbar}\exp(-\kappa_2 z)=\Omega_2\exp(-\kappa_2 z), \tag{15}$$

and the detunings taking into account the Doppler shifts,

$$\tilde{\Delta}_1=\Delta_1-\mathbf{k}_1\cdot\mathbf{v}, \tag{16}$$

$$\tilde{\Delta}_2=\Delta_2-\mathbf{k}_2\cdot\mathbf{v}, \tag{17}$$

$$\tilde{\Delta}_0=\tilde{\Delta}_1+\tilde{\Delta}_2=\Delta_0-(\mathbf{k}_1+\mathbf{k}_2)\cdot\mathbf{v}. \tag{18}$$

We have introduced the following notations: $\Delta_1=\omega_1-\omega_{ig}$, $\Delta_2=\omega_2-\omega_{ei}$, $\Delta_0=\Delta_1+\Delta_2$, and γ_j and γ_{jk} are the respective relaxation rates. In Eqs. (14) and (15), it is necessary to set $\kappa_j=0$ if the corresponding wave is the volume one.

The system of differential equations (8)–(13) should be complemented by boundary conditions. One can divide the ensemble of atoms within the EW field into two parts, namely the atoms approaching the surface and the atoms departing from it. The state of each part is determined by its

own boundary conditions. It is reasonable to assume that Na atoms are adsorbed at a glass surface with unity probability and leave it in their ground state with the polarization quenched at all transitions. These conditions can be written as follows:

$$\sigma_{jk}^{+}(z=0,\mathbf{v})=\delta_{jk}\delta_{jg}, \tag{19}$$

where the superscript ''+'' denotes the atoms departing from the surface with $v_z>0$. For the atoms approaching the surface, we require that the corresponding density-matrix elements be finite at infinite distance from the surface. We thus have the following conditions:

$$|\sigma_{jk}^{-}(z\to\infty,\mathbf{v})|<\infty, \tag{20}$$

where the superscript ''−'' has been set for the atoms approaching the surface with $v_z<0$. The intensity of fluorescence from the upper excited state $|e\rangle$ is determined by the state population averaged over the ensemble of atoms, n_e,

$$n_e=n_e^{-}+n_e^{+}, \tag{21}$$

where

$$n_e^{\pm}=NS\int_0^{\infty}\int dz\, d\mathbf{v} f^{\pm}(\mathbf{v})\sigma_{ee}^{\pm}(z,\mathbf{v}) \tag{22}$$

with N the number density of atoms, S the square on the prism surface where the EW and VW fields intersect each other, and $f^{\pm}$ the velocity distribution functions for the atoms arriving at the surface and desorbing from it. Under the conditions of our experiment, the function f^{-} is dictated by the source of Na atoms. The function f^{+} is determined by the thermodynamic equilibrium of the desorbing atoms with the surface and can be written as (see also Ref. [11])

$$f^{+}(\mathbf{v})=\frac{2}{\pi v_T^4}v_z\exp\left(-\frac{v^2}{v_T^2}\right) \tag{23}$$

with v_T the most probable thermal velocity defined by the surface temperature.

B. The perturbation approach

We suppose that wave 2 does not saturate the upper transition $i\to e$. In such a case, one can apply the perturbation approach with respect to the field amplitude of wave 2. The corresponding equations formally coincide with the equations derived in Ref. [11] if one takes into account that one of the exciting waves is the volume one.

Let us introduce the Laplace-transformed quantities

$$\hat{\sigma}_{jk}(p)=\int_0^{\infty}dz\, e^{-pz}\sigma_{jk}(z). \tag{24}$$

Performing the Laplace transform of the perturbation approach equations, we get the following system of equations with respect to the quantities $\hat{\sigma}_{jk}(p)$:

$$pv_z\hat{\sigma}_{ii}^{(0)}(p)-v_z\sigma_{ii}^{(0)}(0)=-\gamma_i\hat{\sigma}_{ii}^{(0)}(p)+\frac{i}{2}\Omega_1[\hat{\sigma}_{gi}^{(0)}(p+\kappa_1)-\hat{\sigma}_{ig}^{(0)}(p+\kappa_1)], \tag{25}$$

$$pv_z\hat{\sigma}_{ig}^{(0)}(p)-v_z\sigma_{ig}^{(0)}(0)=(i\tilde{\Delta}_1-\gamma_{ig})\hat{\sigma}_{ig}^{(0)}(p)+\frac{i}{2}\Omega_1\left(\frac{1}{p+\kappa_1}-2\theta_{ii}(p)\hat{\sigma}_{ii}^{(0)}(p)\right), \tag{26}$$

$$pv_z\hat{\sigma}_{ei}^{(1)}(p-\kappa_2)-v_z\sigma_{ei}^{(1)}(0)=(i\tilde{\Delta}_2-\gamma_{ei}+\kappa_2 v_z)\hat{\sigma}_{ei}^{(1)}(p-\kappa_2)-\frac{i}{2}\Omega_1\hat{\sigma}_{eg}^{(1)}(p+\kappa_1)+\frac{i}{2}\Omega_2\hat{\sigma}_{ii}^{(0)}(p), \tag{27}$$

$$pv_z\hat{\sigma}_{eg}^{(1)}(p-\kappa_2)-v_z\sigma_{eg}^{(1)}(0)=(i\tilde{\Delta}_0-\gamma_{eg}+\kappa_2 v_z)\hat{\sigma}_{eg}^{(1)}(p-\kappa_2)-\frac{i}{2}\Omega_1\theta_{ei}(p)\hat{\sigma}_{ei}^{(1)}(p-\kappa_2)+\frac{i}{2}\Omega_2\hat{\sigma}_{ig}^{(0)}(p), \tag{28}$$

$$pv_z\hat{\sigma}_{ee}^{(2)}(p-2\kappa_2)-v_z\sigma_{ee}^{(2)}(0)=-(\gamma_e-2\kappa_2 v_z)\hat{\sigma}_{ee}^{(2)}(p-2\kappa_2)+\frac{i}{2}\Omega_2[\hat{\sigma}_{ie}^{(1)}(p-\kappa_2)-\hat{\sigma}_{ei}^{(1)}(p-\kappa_2)]. \tag{29}$$

The caret above a symbol denotes the Laplace transformation of the corresponding quantity, the superscripts in brackets indicate the order of the perturbation approach, and the quantities $\sigma_{jk}^{(n)}(0)$ are the matrix elements $\sigma_{jk}^{(n)}$ taken at $z=0$, which have to be determined from the boundary conditions. We have formally introduced the functions

$$\theta_{ii}(p)=\frac{\hat{\sigma}_{ii}^{(0)}(p+\kappa_1)}{\hat{\sigma}_{ii}^{(0)}(p)} \tag{30}$$

and

$$\theta_{ei}(p)=\frac{\hat{\sigma}_{ei}^{(1)}(p+\kappa_1-\kappa_2)}{\hat{\sigma}_{eg}^{(1)}(p-\kappa_2)}. \tag{31}$$

Equations (25)–(29) are solved to obtain

$$\hat{\sigma}_{ii}^{(0)}(p)=\frac{\Omega_1^2}{2(p+2\kappa_1)}\frac{\Gamma_{ig}(p)}{\Gamma_i(p)}\frac{1}{\tilde{\Delta}_1^2+\Gamma_1^2(p)}+\frac{v_z}{\Gamma_i(p)}\frac{\tilde{\Delta}_1^2+\Gamma_{ig}^2(p)}{\tilde{\Delta}_1^2+\Gamma_1^2(p)}\left\{\sigma_{ii}^{(0)}(0)+\frac{\Omega_1}{2}\left(\frac{\sigma_{ig}^{(0)}(0)}{\tilde{\Delta}_1+i\Gamma_{ig}(p)}+\text{c.c.}\right)\right\}, \tag{32}$$

$$\hat{\sigma}_{ig}^{(0)}(p+\kappa_1)=i[\tilde{\Delta}_1+i\Gamma_{ig}(p)]^{-1}\left(\frac{i}{2}\frac{\Omega_1}{p+2\kappa_1}-i\Omega_1\pi_{ii}(p)\hat{\sigma}_{ii}^{(0)}(p)+v_z\sigma_{ig}^{(0)}(0)\right), \tag{33}$$

$$\hat{\sigma}_{ei}^{(1)}(p-\kappa_2)=-\{[\tilde{\Delta}_2+i\Gamma_{ei}(p)][\tilde{\Delta}_0+i\Gamma_{eg}(p)]-\tfrac{1}{4}\pi_{ei}(p)\Omega_1^2\}^{-1}\left\{\tfrac{1}{2}\Omega_2[\tilde{\Delta}_0+i\Gamma_{eg}(p)]\times\hat{\sigma}_{ii}^{(0)}(p)+\tfrac{1}{4}\Omega_1\Omega_2\hat{\sigma}_{ig}^{(0)}(p+\kappa_1)-iv_z[\tilde{\Delta}_0+i\Gamma_{eg}(p)]\sigma_{ei}^{(1)}(0)-\frac{i}{2}v_z\Omega_1\sigma_{eg}^{(1)}(0)\right\}, \tag{34}$$

$$\hat{\sigma}_{ee}^{(2)}(p-2\kappa_2)=\frac{1}{\Gamma_e(p)}\left\{\frac{i}{2}\Omega_2[\hat{\sigma}_{ie}^{(1)}(p-\kappa_2)-\hat{\sigma}_{ei}^{(1)}(p-\kappa_2)]+v_z\sigma_{ee}^{(2)}(0)\right\}. \tag{35}$$

We have introduced the following functions:

$$\Gamma_i(p)=\gamma_i+pv_z, \tag{36}$$

$$\Gamma_e(p)=\gamma_e+(p-2\kappa_2)v_z, \tag{37}$$

$$\Gamma_{ig}(p)=\gamma_{ig}+(p+\kappa_1)v_z, \tag{38}$$

$$\Gamma_{ei}(p)=\gamma_{ei}+(p-\kappa_2)v_z, \tag{39}$$

$$\Gamma_{eg}(p)=\gamma_{eg}+(p+\kappa_1-\kappa_2)v_z, \tag{40}$$

which denote the relaxation rates taking into account the time-of-flight broadening in the EW fields, and

$$\Gamma_1(p)=\Gamma_{ig}(p)\sqrt{1+\frac{\pi_{ii}(p)\Omega_1^2}{\Gamma_i(p)\Gamma_{ig}(p)}}, \tag{41}$$

which characterizes the power broadening of the lower transition. The functions

$$\pi_{ii}(p)=\theta_{ii}(p)\,\theta_{ii}(p+\kappa_1)=\frac{\hat{\sigma}_{ii}^{(0)}(p+2\kappa_1)}{\hat{\sigma}_{ii}^{(0)}(p)} \tag{42}$$

and

$$\pi_{ei}(p)=\theta_{ei}(p)\,\theta_{ei}(p+\kappa_1)=\frac{\hat{\sigma}_{ei}^{(1)}(p+2\kappa_1-\kappa_2)}{\hat{\sigma}_{ei}^{(1)}(p-\kappa_2)} \tag{43}$$

determine the power broadening and Stark splitting of the lower transition, respectively [14]. For the normal configuration, one has to set $\kappa_1=0$ in all equations. In this case, we have $\pi_{ii}(p)=\pi_{ei}(p)=1$. For the inverse configuration, $\kappa_2=0$. Then the functions $\pi_{ii}(p)$ and $\pi_{ei}(p)$ effectively take into account the evanescent character of wave 1.

The functions $\pi_{ii}(p)$ and $\pi_{ei}(p)$ are expressed in terms of the solutions themselves. In principle, the corresponding equations can be solved by an iterative procedure. On the other hand, one can apply various approximations for their calculation (see Ref. [11]).

Now the excited-state populations defined by Eq. (22) in the lowest nonvanishing order can be determined as follows:

$$n_e^{\pm}=NS\int d\mathbf{v}f^{\pm}(\mathbf{v})\hat{\sigma}_{ee}^{\pm(2)}(0,\mathbf{v}). \tag{44}$$

1. Contribution of desorbing atoms

Let us now take into account the boundary conditions (19) for the desorbing atoms in the expressions (32)–(35). We then get solutions that formally coincide with those derived in Ref. [11]. We present here the result (we omit the superscripts ''+'' for the sake of brevity)

$$\hat{\sigma}_{ee}^{(2)}(p-2\kappa_2)=\frac{\Omega_2}{\Gamma_e(p)}\text{Im}[\hat{\sigma}_{ei}^{(1)}(p-\kappa_2)], \tag{45}$$

where

$$\hat{\sigma}_{ei}^{(1)}(p-\kappa_2)=-\frac{\Omega_1^2\Omega_2}{8(p+2\kappa_1)}\frac{\Gamma_{ig}(p)}{\Gamma_i(p)}\frac{1}{\tilde{\Delta}_1^2+\Gamma_1^2(p)}\times\frac{2[\tilde{\Delta}_0+i\Gamma_{eg}(p)]-[\Gamma_i(p)/\Gamma_{ig}(p)][\tilde{\Delta}_1-i\Gamma_{ig}(p)]}{[\tilde{\Delta}_2+i\Gamma_{ei}(p)][\tilde{\Delta}_0+i\Gamma_{eg}(p)]-(1/4)\pi_{ei}(p)\Omega_1^2}. \tag{46}$$

2. Contribution of arriving atoms

In this case, the arbitrary constants $\sigma_{jk}^{(n)}(0)$ must be chosen such that all the solutions $\sigma_{jk}^{(n)}(z)$ are finite at infinite distance from the surface. As the functions $\pi_{ii}(p)$ and $\pi_{ei}(p)$ are continuous [11], the Weierstrass theorem [15] allows us to approximate them by polynomials in p with an arbitrary small error. Then the obtained solutions for the Laplace-transformed quantities $\hat{\sigma}_{jk}^{(n)}(p)$ can be represented as sums of rational functions $F(p)$. According to the Heaviside expansion theorem [16], the corresponding original functions have the form of a sum of exponents $\exp(p_nz)$ weighted by coefficients that are equal to the residues of the $F(p)$ in the poles p_n. Thus only negative poles will give a contribution to the original function, which is finite at $z\to\infty$. For the atoms arriving at the surface, $v_z<0$, and to ensure the finite-

ness of the solutions for *all* possible values of atomic velocities, laser detunings, and intensities, one has to leave only the terms having a pole at $p=-2\kappa_1$. All the other terms should be canceled by an appropriate choice of the constants $\sigma_{jk}^{(n)}(0)$. The final solution can be formally obtained from Eqs. (45) and (46) if all the quantities $\Gamma_j(p)$, $\Gamma_{jk}(p)$, $\pi_{ii}(p)$, and $\pi_{ei}(p)$ are taken at $p=-2\kappa_1$.

C. The weak-field limit

To understand qualitatively what spectra can be observed in different configurations, let us consider first the case in which both waves can be treated as weak, i.e., nonsaturating in the corresponding transitions. The weak-field limit can be obtained from Eqs. (45) and (46) if one neglects the terms proportional to Ω_1^2 in the denominator of the $\hat{\sigma}_{ei}^{(1)}(p-\kappa_2)$, namely

$$\hat{\sigma}_{ei}^{(1)}(p-\kappa_2) = -\frac{\Omega_1^2\Omega_2}{8(p+2\kappa_1)}\frac{\Gamma_{ig}(p)}{\Gamma_i(p)}\frac{1}{\tilde{\Delta}_1^2+\Gamma_{ig}^2(p)} \times\frac{2[\tilde{\Delta}_0+i\Gamma_{eg}(p)]-[\Gamma_i(p)/\Gamma_{ig}(p)][\tilde{\Delta}_1-i\Gamma_{ig}(p)]}{[\tilde{\Delta}_2+i\Gamma_{ei}(p)][\tilde{\Delta}_0+i\Gamma_{ei}(p)]}. \quad (47)$$

Let us suppose that near the critical angle, the time-of-flight broadening can be neglected in comparison with the natural linewidths, which in turn are much smaller than the Doppler widths of the corresponding transitions. Then from Eqs. (46) and (45) we get the following result:

$$\hat{\sigma}_{ee}^{(2)}(p-2\kappa_2)=\frac{\pi^2}{8}\frac{\Omega_1^2\Omega_2^2}{\gamma_i\gamma_e}\frac{1}{p+2\kappa_1}\delta(\tilde{\Delta}_1)\delta(\tilde{\Delta}_2), \quad (48)$$

where $\delta(x)$ is the Dirac delta function.

The exited-state populations (44) can now be obtained easily. In the normal configuration, we get

$$n_e^+=Af^+\left(\frac{\Delta_2}{k_2},\frac{\Delta_1}{k_1}\right)\Theta(\Delta_1), \quad (49)$$

$$n_e^-=Af^-\left(\frac{\Delta_2}{k_2},\frac{\Delta_1}{k_1}\right)[1-\Theta(\Delta_1)], \quad (50)$$

where

$$A=NS\frac{\pi^2}{16}\frac{\Omega_1^2\Omega_2^2}{(\kappa_1+\kappa_2)k_1k_2\gamma_i\gamma_e} \quad (51)$$

and $\Theta(x)$ is the unit step function.

In the inverse configuration,

$$n_e^+=Af^+\left(\frac{\Delta_1}{k_1},\frac{\Delta_2}{k_2}\right)\Theta(\Delta_2) \quad (52)$$

and

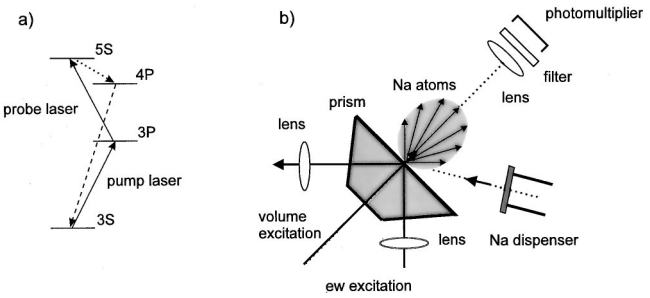

FIG. 3. (a) Term scheme of sodium, relevant for the two-photon excitation process. Hyperfine splitting is not indicated. (b) The experimental setup. The lasers for volume excitation and EW (evanescent wave) excitation are exchangable, as indicated in Fig. 2. The photomultiplier detects radiation via filters solely from the $4P\rightarrow 3S$ optical transition in Na.

$$n_e^-=Af^-\left(\frac{\Delta_1}{k_1},\frac{\Delta_2}{k_2}\right)[1-\Theta(\Delta_2)]. \quad (53)$$

Here, the reduced velocity distribution function $f(v_x,v_z)$ has been introduced since the density matrix does not depend on the v_y component. Thus we conclude that in the normal configuration, when Δ_2 is varying, one scans the distribution function of atomic velocities along the surface. For positive laser 1 detunings, the spectrum is determined by the contribution of atoms moving away from the surface, whereas for negative detunings it is determined by the atoms arriving at the surface. In the inverse configuration, one scans the distribution function of atomic velocities along the normal to the surface. In this case, the atoms departing from the surface contribute to the right wing of the spectrum, whereas the atoms arriving at the surface contribute to the left wing.

Let us now consider the case in which the velocity distribution function $f(\mathbf{v})=f(v,\theta)$ has a narrow peak at some definite angle θ_0. Here, the angle θ characterizes the direction of the atomic velocity. The product of the δ functions that determines the spectrum can be transformed as

$$\delta(\tilde{\Delta}_1)\delta(\tilde{\Delta}_2)\sim\delta\left(v-\frac{\Delta_1}{k_1\cos\theta}\right)\delta\left(\Delta_2-\frac{k_2}{k_1}\Delta_1\cot\theta\right), \quad (54)$$

where we have chosen as θ the angle between the velocity vector and the vector $\mathbf{k}_1$. It follows from that expression that upon scanning of the detuning Δ_2, fluorescence intensity will be observed essentially only in the narrow vicinity of the detuning,

$$\Delta_2^m=\frac{k_2}{k_1}\Delta_1\cot\theta_0. \quad (55)$$

III. EXPERIMENTAL SETUP

The experimental setup is shown in Fig. 3. A truncated glass prism [17] is mounted on a manipulator in a high vacuum ($p_0\leqslant 10^{-8}$ mbar) chamber. It can be heated resistively up to 445 K and cooled via liquid nitrogen. The light of two frequency tunable, single-mode ring dye lasers is

transferred into the apparatus via glass windows and optical fibers. The fibers allow us to easily exchange the volume vs evanescent wave contribution of pump and probe lasers and also to accomplish *p* polarization by the use of Glan polarizers. The total linewidth of both lasers is about 3 MHz with a measured drift of far less than 90 MHz during a typical wavelength scan. The diameters of the laser beams at the surface are 0.5 mm (laser 1) and 2 mm (laser 2), respectively, and laser powers of up to 60 mW each are used.

An evanescent wave is excited by one of the lasers at the glass prism surface at an angle in the vicinity of the critical angle for total internal reflection. The second laser generates a volume wave, which propagates perpendicular to the prism surface via the truncated apex of the prism towards the vacuum side. While laser 1 is resonant to the $3S_{1/2} \leftarrow 3P_{3/2}$ Na atomic transition (16 973.33 cm^{-1}), the other one (laser 2) is scanned around the $3P_{3/2} \leftarrow 5S_{1/2}$ resonance transition (16 227.30 cm^{-1}). The starting frequency (''0'' on the frequency axis in Figs. 4–10) corresponds to 16 227.2741 cm^{-1}, as determined by an iodine absorption cell. The blueshifted fluorescence light from the $4P_{1/2,3/2} \rightarrow 3S_{1/2}$ transitions (30 267.28 cm^{-1} and 30 272.88 cm^{-1}) is observed via a collection lens at normal incidence and is recorded behind a glass (Schott UG5) and an interference filter ($\Delta\lambda = 10$ nm) by a photomultiplier and photon-counting electronics.

A flux of about 5×10^{15} sodium atoms per second from a Na dispenser (SAES getters) reaches the prism surface at an angle $\theta_0 = 55 \pm 5°$ with respect to the surface normal. The flux is directed in the plane of incidence of the laser beam exciting the EW along its propagation direction. It determines the velocity distribution function of the atoms arriving at the surface.

IV. RESULTS AND DISCUSSION

Two-photon fluorescence spectra obtained in the normal configuration are shown in Figs. 4 and 5. For negative detuning of laser 1, a narrow peak is observed besides the Doppler-broadened line whose position changes with the detuning Δ_1. For positive laser 1 detunings, the intensity of the narrow peak essentially decreases. In the inverse configuration (Figs. 6, 7, and 8) the narrow peak also can be observed, but this time at the left-wing side of the Doppler-broadened line. For negative detunings of laser 1, the narrow peak disappears. In this case, in contrast to the normal configuration, a clear two-peak shape of the broad fluorescence line is observed. The separation between the two maxima depends neither on the intensity of laser 1 (Fig. 9) nor its detuning (Fig. 10).

Based on the theoretical results obtained for the weak-field limit (Sec. II C), one can identify contributions of different groups of atoms near the surface. In accordance with the previous statements, we conclude that the narrow peak arises from the atoms emanating from the dispenser, which have a narrow velocity distribution around a definite angle. Plotting the position of this peak, Δ_2^m, as a function of the detuning of laser 1, Δ_1, we get a linear dependence (Fig. 11), in agreement with Eq. (55). From its slope we determine the value $\theta_0 = 53 \pm 2°$, within error bars in agreement with the measured value.

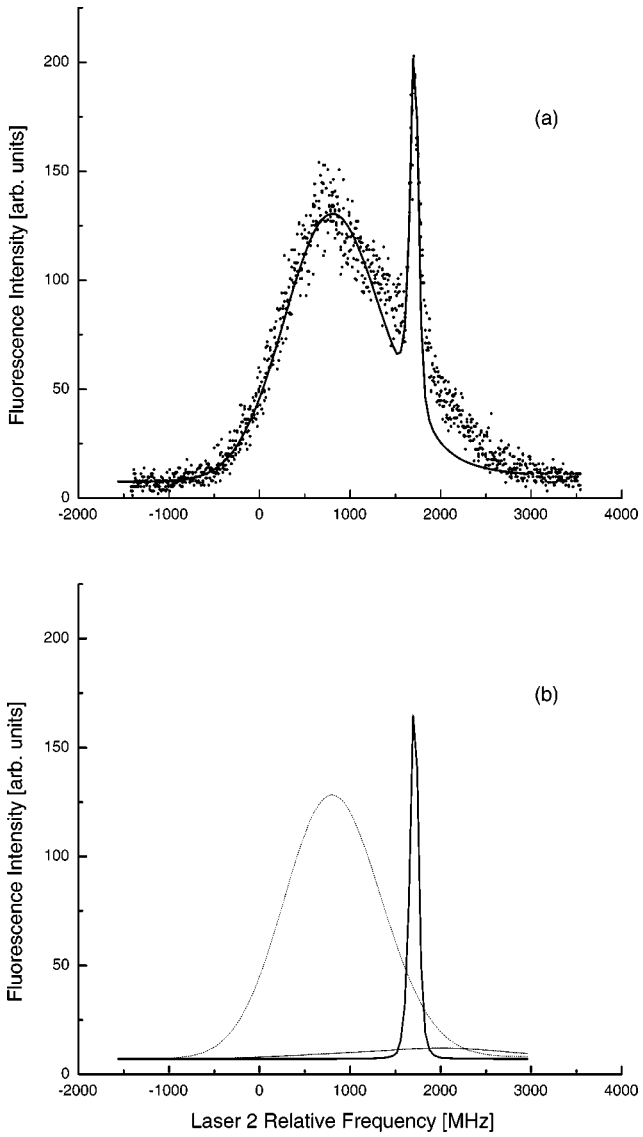

FIG. 4. (a) Two-photon fluorescence spectra observed in the ''normal configuration'' (dots). Laser 1 power $P_1 = 15$ mW, laser 2 power $P_2 = 15$ mW, and $\Delta_1 = -800$ MHz; surface temperature $T = 396$ K. The fit (solid line) is obtained for a Rabi frequency for the lower transition $\Omega_1/(2\pi) = 90.5$ MHz and for an EW penetration depth $\delta = 196$ μm. The contributions of different groups of atoms are shown separately in (b): the atoms flying directly from the dispenser (solid line), the atoms scattered before the surface (dashed line), and the atoms desorbed from the surface (dash-dotted line).

In the normal configuration for negative Δ_1 one observes the contribution of the atoms arriving at the surface. The same is true for the left wing of the spectrum obtained in the inverse configuration. However, besides a narrow peak from the dispenser, one can also see a Doppler-broadened contribution. This observation reveals that the atoms emitted by the dispenser have undergone collisions with each other before they reach the surface. This is consistent with the fact that the distance between the dispenser and the surface (3 cm) is comparable with the mean free path of sodium atoms

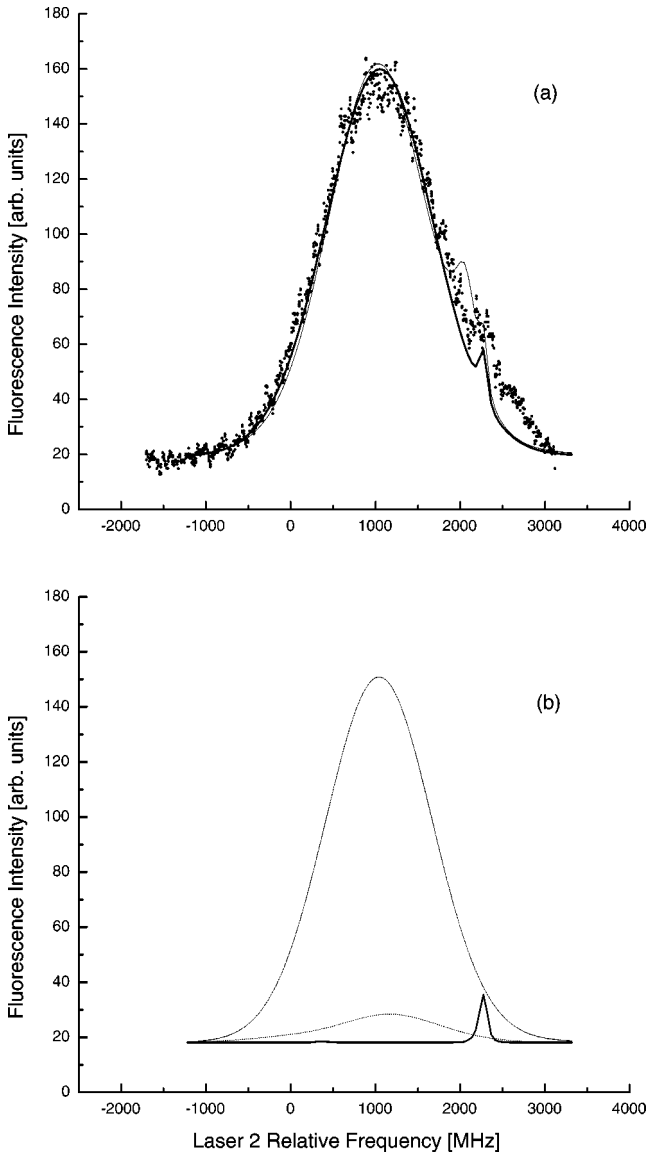

FIG. 5. Same as Fig. 4, but for $\Delta_1 = 800$ MHz, $T = 399$ K. In (a) two calculated spectra are presented: the sticking probability for $s = 1$ (thick solid line) and for $s = 0.5$ (thin solid line).

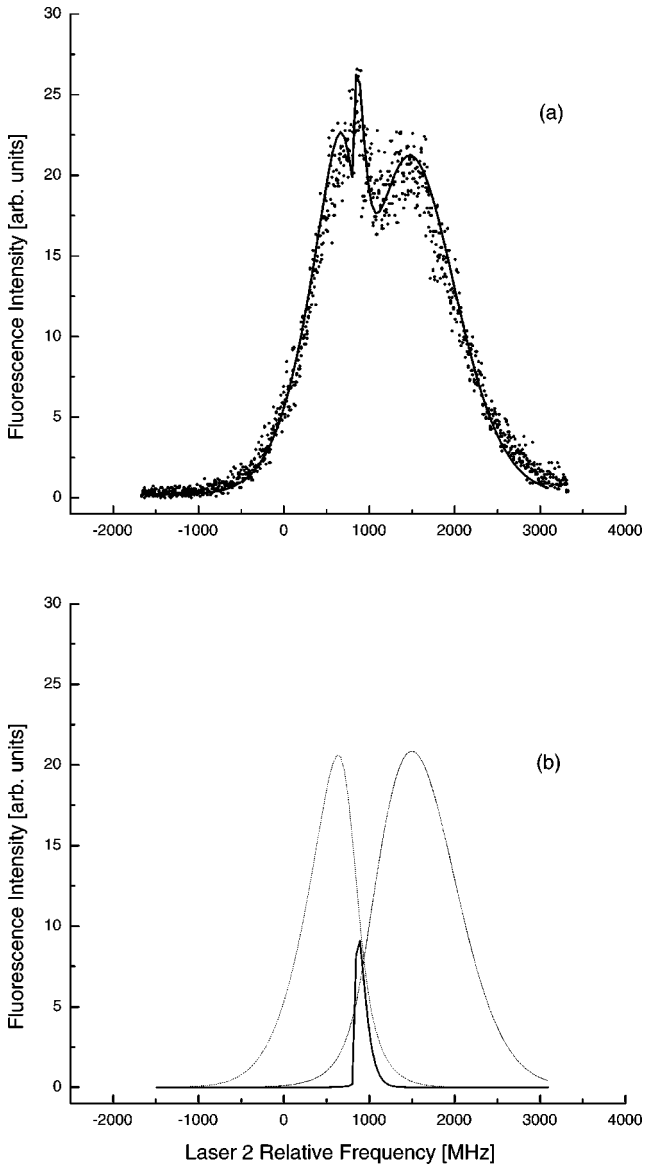

FIG. 6. Two-photon fluorescence spectra observed in the ''inverse configuration'' (dots) at $P_1 = 53$ mW and $P_2 = 15$ mW and $T = 407$ K: $\Delta_1 = 0$ MHz. The fits (solid lines) are obtained for $\Omega_1/(2\pi) = 275$ MHz, $\delta = 196$ μm, $\pi_{ii} = 1$, and $\pi_{ei} = 0.01$. The other notations are as in Fig. 4.

from the source (4 cm).

To confirm this conclusion in a more direct way, we have measured the one-photon fluorescence spectrum of the atomic flux emitted from the dispenser in a cell. The corresponding spectra excited both in the direction along the dispenser axis and perpendicular to it are shown in Fig. 12. The spectrum excited along the dispenser axis [Fig. 12(a)] is compared with the Maxwellian velocity distribution taking into account the flux correction

$$f_{\parallel}(v_{\parallel}) = \frac{2}{v_d^2} v_{\parallel} \exp\left(- \frac{v_{\parallel}^2}{v_d^2} \right), \tag{56}$$

where $v_{\parallel}$ is the velocity component along the dispenser axis and $v_d = 8.0 \times 10^4$ cm/s is the most probable velocity determined by the temperature of the dispenser, $T_d = 900$ K [18].

To fit the spectrum excited perpendicular to the dispenser axis [Fig. 12(b)], we have used a sum of Lorentzian and Gaussian curves,

$$f_{\perp}(v_{\perp}) = \frac{1}{C} \left[\frac{w}{\pi} \frac{1}{v_{\perp}^2 + w^2} + p \frac{1}{\sqrt{\pi} u} \exp\left(- \frac{v_{\perp}^2}{u^2} \right) \right], \tag{57}$$

where $v_{\perp}$ is the velocity component perpendicular to the dispenser axis, C is the normalization constant, and the quantities w, u, and p are fitting parameters. The best fit was obtained for $w = 1.1 \times 10^4$ cm/s, $u = 4.4 \times 10^4$ cm/s, and $p = 0.5$. For both experimental configurations, all the hyperfine levels have been taken into account for the fit and the two peaks correspond to the two hyperfine components of the

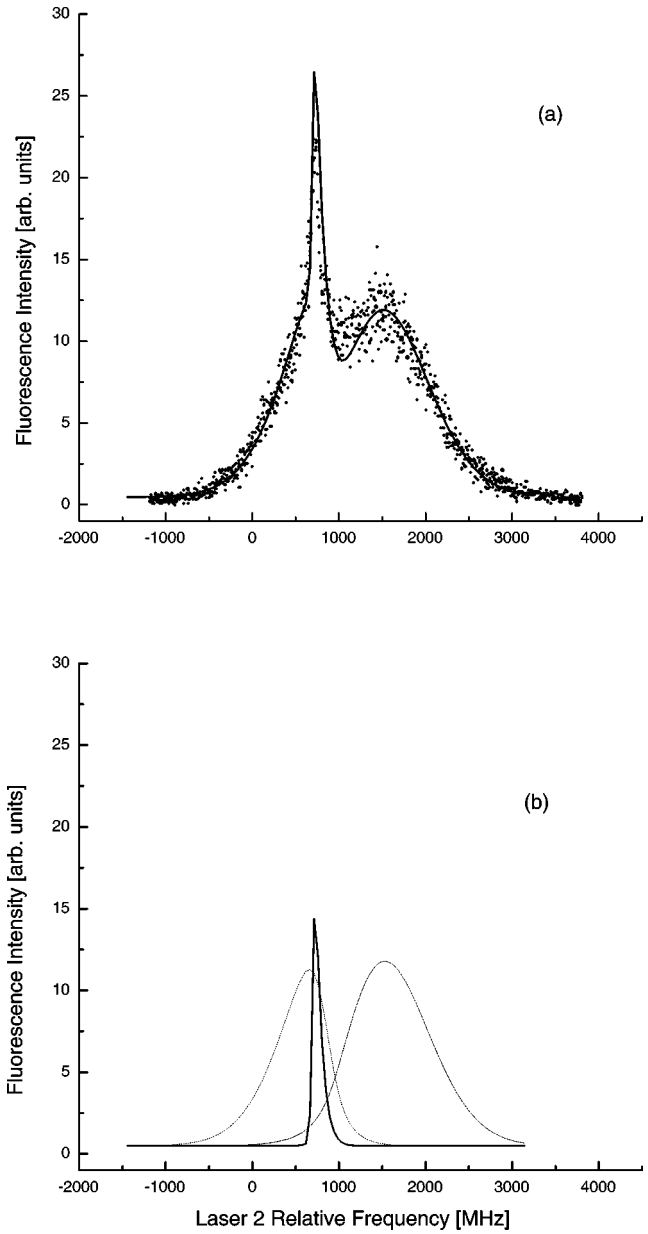

FIG. 7. Same as Fig. 6, but for $\Delta_1 = 200$ MHz.

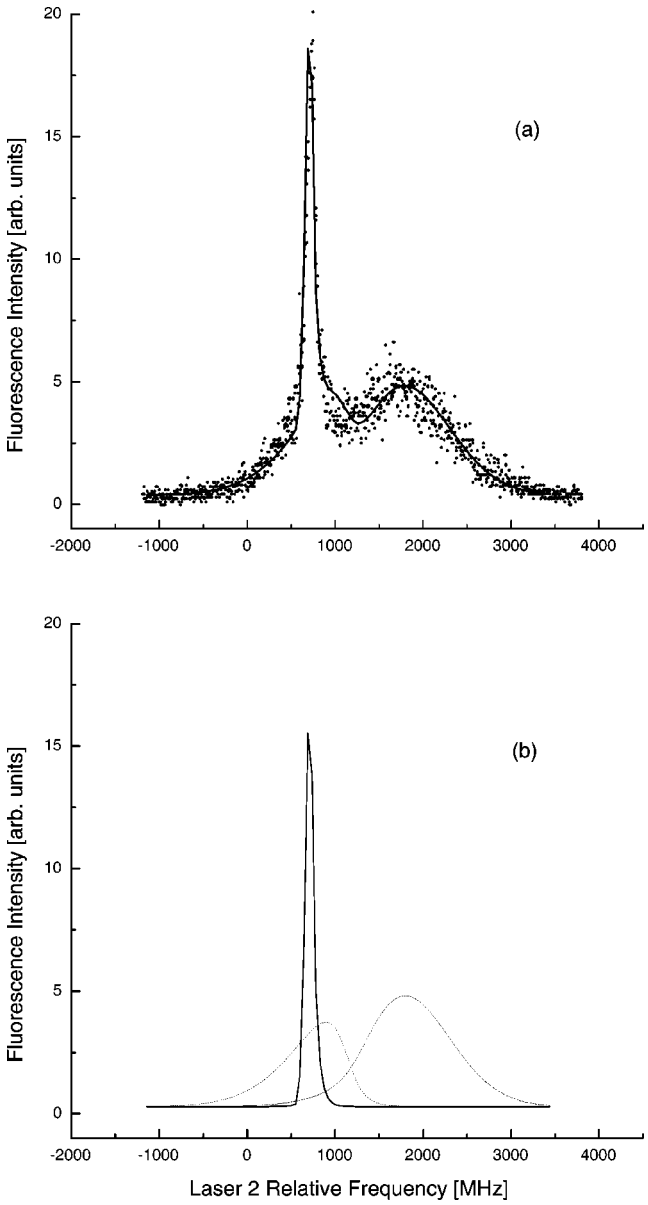

FIG. 8. Same as Fig. 6, but for $\Delta_1 = 600$ MHz.

ground state $3S_{1/2}$. A small discrepancy between the measured and calculated spectra in Fig. 12(b) can be explained by a slight misalignment of the perpendicular orientation of the laser beam with respect to the dispenser axis. The narrow Lorentzian line can be identified as arising from the atoms emitted directly from the dispenser. The broader Gaussian background originates from the atoms that have undergone mutual collisions. Thus the parameter p is connected with the probability of such collisions.

Next we have performed a quantitative analysis of the measured two-photon fluorescence spectra by applying the rigorous theory developed in Sec. II B. As input for the fitting procedure, we have used the velocity distribution functions obtained from the one-photon fluorescence spectra in a cell. Namely, for the contribution of collision-free atoms from the dispenser, we have used the distribution function

$$f_d(v_\parallel, v_\perp) = \frac{1}{C_d} \frac{v_\parallel}{v_\perp^2 + w^2} \exp\left(- \frac{v_\parallel^2}{v_d^2} \right) \tag{58}$$

with the normalization constant C_d. For the atoms that have undergone collisions in front of the surface, we have taken a Maxwellian distribution,

$$f_{ds}(v) = \frac{1}{\pi u^2} \exp\left(- \frac{v^2}{u^2} \right) \tag{59}$$

with the parameter u as determined above. Finally, for the atoms desorbed from the surface we have used the distribution function (23) reduced to the plane (v_x, v_z). The ratios between the contributions of different groups of atoms as

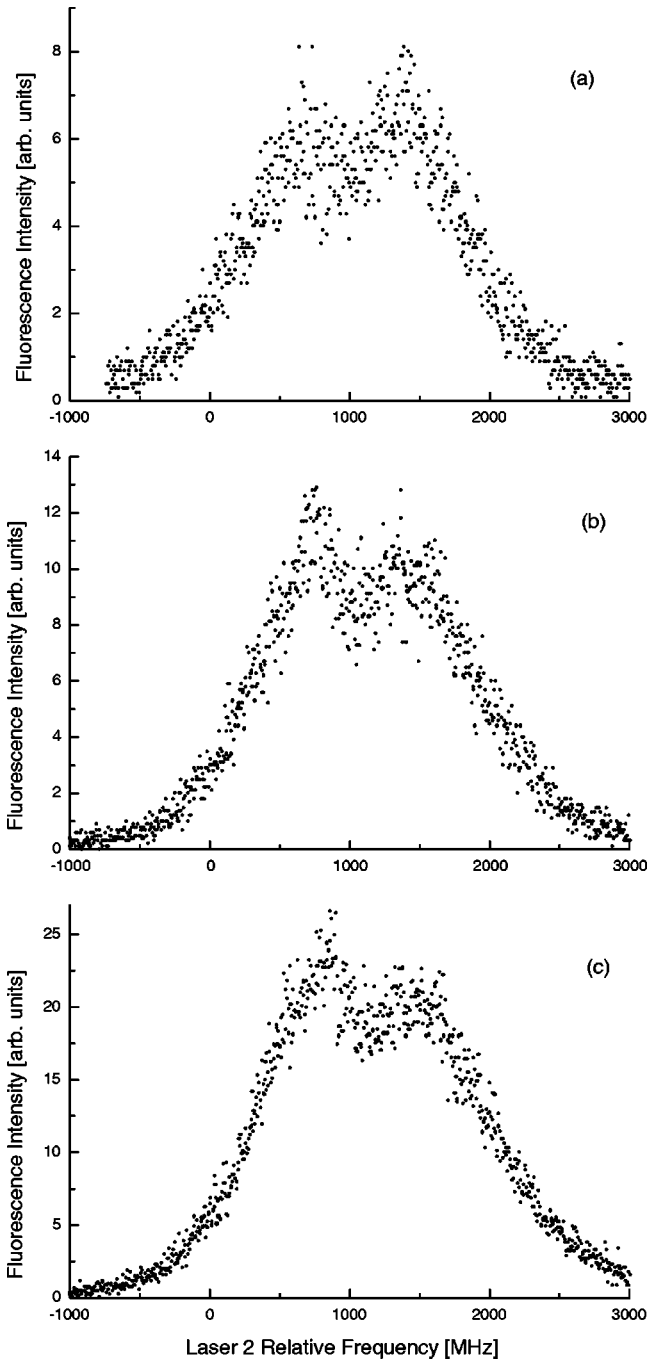

FIG. 9. Dependence of the observed two-photon spectra on the intensity of laser 1, obtained in the inverse configuration. (a) 15 mW, (b) 38 mW, (c) 53 mW.

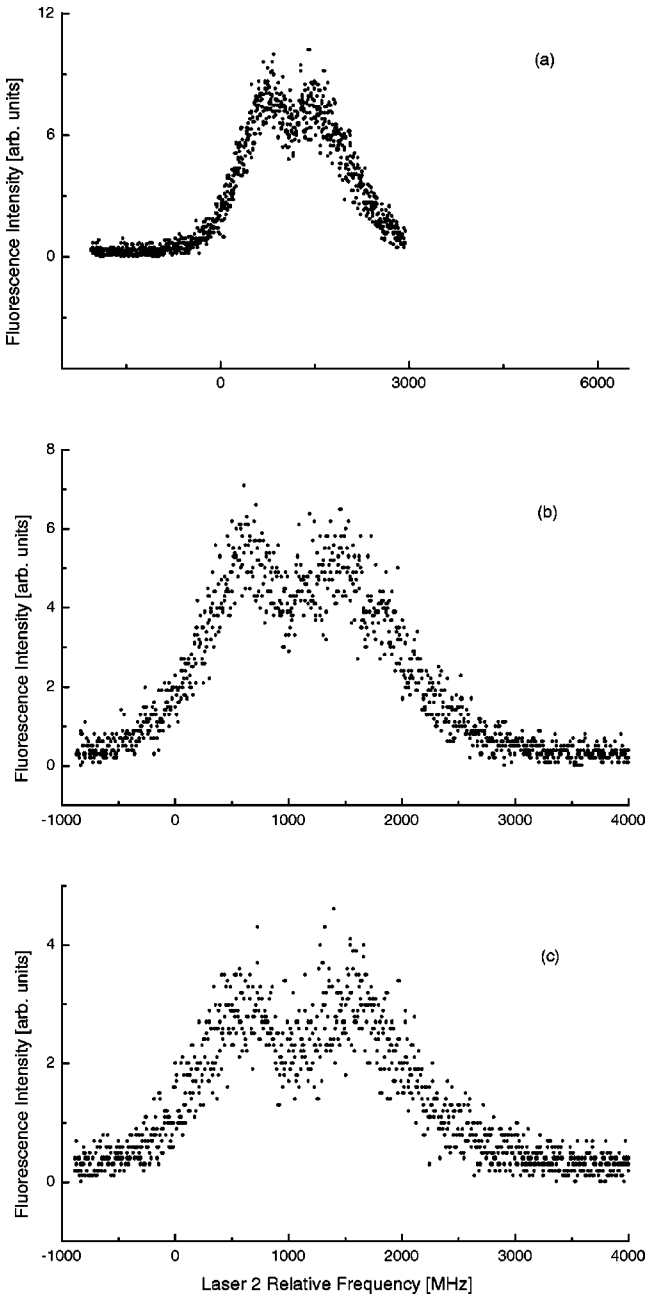

FIG. 10. Dependence of the two-photon spectra on the detuning of laser 1, obtained in the inverse configuration. (a) $\Delta_1 = -200$ MHz, (b) $\Delta_1 = -400$ MHz, (c) $\Delta_1 = -600$ MHz.

well as the quantities π_{ii}, π_{ei} (in the inverse configuration) and the EW penetration depth were considered as adjustable parameters.

The results of numerical calculations are shown in Figs. 4–8. First, a fit was obtained for a single spectrum in the inverse configuration (Fig. 6) and then the other spectra were calculated using the measured values of the detuning of laser 1, keeping all other parameters constant. For the calculations of the spectra in the normal configuration, only the intensity of wave 1 was assumed to be different from that in the inverse configuration as it differs between volume and evanescent wave.

A fairly good agreement between calculated and observed spectra confirms that all contributions have been properly identified. A slight discrepancy between theoretical and experimental data in Fig. 4 can be attributed to an asymmetric velocity distribution of the atoms arriving at the surface that have experienced collisions. As the dispenser-surface distance is comparable with the mean free path of Na atoms, their velocity distribution is essentially nonequilibrium and cannot be described by a Maxwellian distribution function. Rather, it can be characterized by a specific direction along

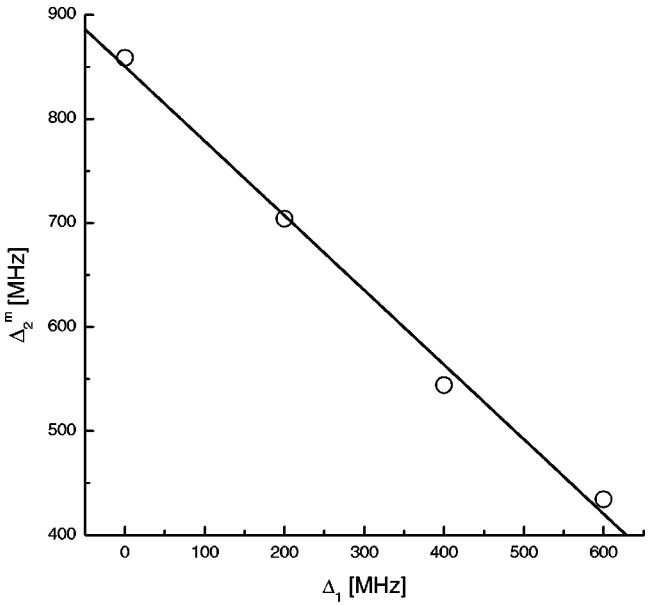

FIG. 11. Dependence of the narrow peak position on the detuning of laser 1 in the inverse configuration.

the dispenser axis. This can also cause the slight discrepancy between experiment and theory in Fig. 5. This spectrum has been obtained for large positive Δ_1, so both hyperfine sublevels of the ground state $3S_{1/2}$ participate in the transition. For one of the sublevels the detuning is negative, so the atoms arriving at the surface also contribute to the spectrum.

A remarkable feature of the Doppler-broadened fluorescence lines is that they are qualitatively different in the normal as compared to the inverse configuration. The dip at the center of the line in the case of the inverse configuration arises from the factor v_z in the velocity distribution function of the atoms desorbed from the surface, which is a consequence of Knudsen's cosine law. In the normal configuration, one scans the velocity distribution along the *x* direction and this factor is not displayed.

Until now we have assumed throughout the paper that the atoms are adsorbed at the surface with a probability of unity. However, in principle there may be a nonzero probability for an atom to be specularly scattered. In such a case, one would observe a narrow line arising from the atoms stemming directly from the dispenser and then specularly scattered by the surface. The spectral position of this line could undoubtedly be identified in the normal configuration with positive detuning of laser 1 [Fig. 5(a)]. From the present data we conclude that the sticking probability for Na atoms under our experimental conditions is larger than 0.5 and probably about unity. This conclusion is consistent with the results of previous measurements [10,19].

V. CONCLUSIONS

We have investigated both theoretically and experimentally the two-photon fluorescence spectra of Na vapor in the close vicinity of a glass prism surface. The Na atoms were excited in a step-by-step excitation scheme in two different configurations: (i) the lower transition is saturated by a volume wave propagating perpendicular to the surface, whereas the upper transition is scanned by an evanescent surface wave, and (ii) the character of the two waves is exchanged. We have developed a rigorous theory describing the resulting fluorescence spectra. Based on our theoretical approach, we were able to identify the spectral contributions of different groups of atoms participating in the vapor-solid scattering. Such spectral separation has allowed us to reconstruct the velocity distribution functions of the specific groups of atoms both in the direction parallel to the surface and perpendicular to it. This new technique provides a spectral distinction between the contributions of the atoms just before they collide with the surface and just after they desorb from it. Moreover, it allows one to identify unambiguously the

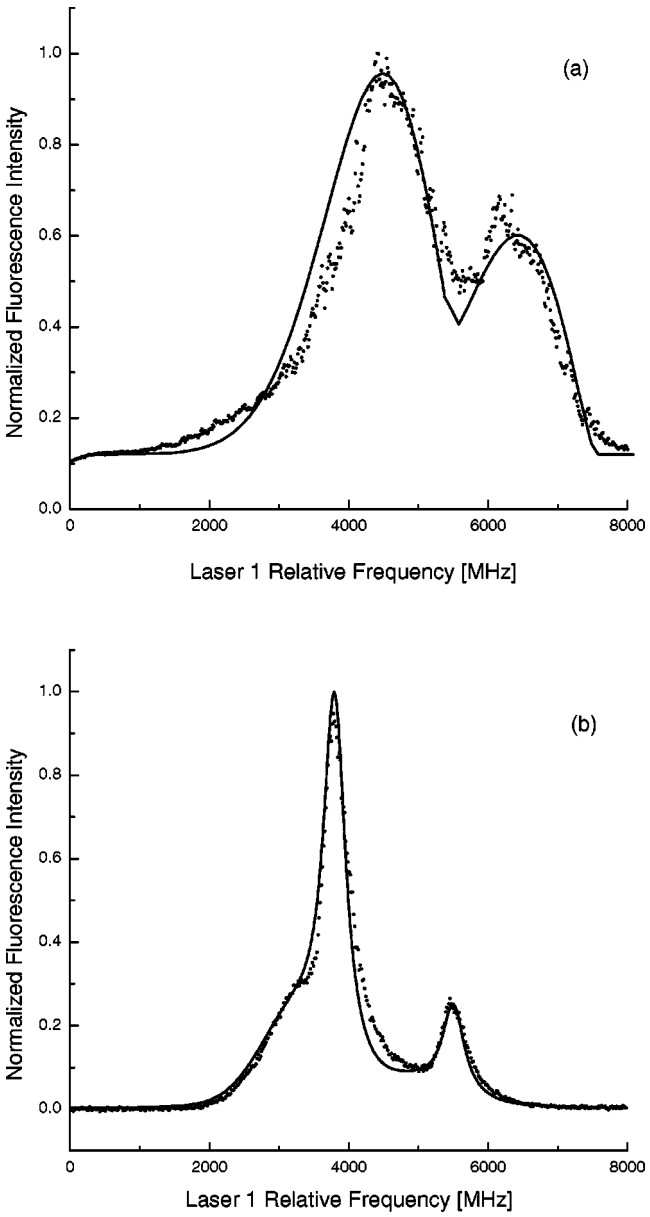

FIG. 12. One-photon fluorescence spectra measured in a cell excited along the dispenser axis (a) and perpendicular to it (b). Note that the ''0'' on the frequency axis is an arbitrary value. The solid lines are fit curves; see text.

spectral contribution of the atoms specularly scattered by the surface, if any.

Once the velocity distribution functions of both atomic fluxes are known, important quantities characterizing the gas-solid boundary layer can be calculated: the scattering kernel and different accommodation coefficients [20]. On the other hand, comparing the molecular fluxes to the surface and apart from it, one can extract information about chemical reactions on the surface [21]. The main criterion for applicability of this technique is that the depth of penetration of the evanescent wave into the gas must be less than the mean free path of the gas atoms. In the visible spectral range, the penetration depth can easily be made less than 1 μm. The mean free path reaches such values at gas pressures of the order of one atmosphere. Therefore, such a technique can bridge the so-called ''pressure gap'' in heterogeneous catalysis [22].

ACKNOWLEDGMENTS

We are grateful to J.P. Toennies for continuous and encouraging support during the experimental part of this work. We also appreciate support from the Danish Natural Science Council.

[1] G. Comsa and R. David, Surf. Sci. Rep. **5**, 145 (1985).
[2] P. Boissel and F. Kerherve, Opt. Commun. **37**, 397 (1981).
[3] P. Simoneau, S. Le Boiteux, C.B. de Araujo, D. Bloch, J.R.R. Leite, and M. Ducloy, Opt. Commun. **59**, 103 (1986).
[4] *Surface Polaritons*, edited by V.M. Agranovich and D.L. Mills (North-Holland, Amsterdam, 1982).
[5] M.F.H. Schuurmans, J. Phys. (Paris) **37**, 469 (1976).
[6] V.G. Bordo, Phys. Lett. A **146**, 447 (1990).
[7] V.G. Bordo, Surf. Sci. **269/270**, 169 (1992).
[8] V.G. Bordo, Opt. Commun. **101**, 37 (1993).
[9] V.G. Bordo, Opt. Commun. **111**, 61 (1994).
[10] V.G. Bordo, C. Henkel, A. Lindinger, and H.-G. Rubahn, Opt. Commun. **137**, 249 (1997).
[11] V.G. Bordo and H.-G. Rubahn, Phys. Rev. A **60**, 1538 (1999).
[12] The one-dimensional velocity distribution function of the atoms along the normal to the surface can also be monitored in selective reflection from the transparent dielectric-vapor interface. See F. Schuller, O. Gorceix, and M. Ducloy, Phys. Rev. A **47**, 519 (1993); and O.A. Rabi, A. Amy-Klein, S. Saltiel, and M. Ducloy, Europhys. Lett. **25**, 579 (1994).
[13] We consider here a closed three-level system. Generalization for the case in which optical pumping takes place can be carried out as in Ref. [11].
[14] This follows from comparison of Eqs. (32) and (34) with analogous results obtained for two-photon excitation by volume waves. See R. Salomaa and S. Stenholm, J. Phys. B **9**, 1221 (1976).
[15] K. Weierstrass, Sitzungsber. Acad. Berlin **40**, 633 (1885).
[16] *Handbook of Mathematical Functions*, edited by M. Abramovitz and I.A. Stegun (Dover Publications, New York, 1972), p. 1021.
[17] Recently a similar setup was used to measure the penetration depth and pseudomomentum of evanescent waves. See T. Matsudo, H. Hori, T. Inoue, H. Iwata, Y. Inoue, and T. Sakurai, Phys. Rev. A **55**, 2406 (1997).
[18] F. Balzer, K. Bammel, and H.-G. Rubahn, J. Chem. Phys. **98**, 7625 (1993).
[19] F. Balzer, M. Hartmann, M. Renger, and H.-G. Rubahn, Z. Phys. D: At., Mol. Clusters **28**, 321 (1993).
[20] C. Cercignani, *The Boltzmann Equation and Its Applications* (Springer-Verlag, New York, 1988), Chap. III.
[21] See also V.G. Bordo, Phys. Status Solidi A **175**, 271 (1999).
[22] H.P. Bonzel, Surf. Sci. **68**, 236 (1977).